Ceramics International xxx (xxxx) xxx–xxx

Contents lists available at ScienceDirect

Ceramics International

journal homepage: www.elsevier.com/locate/ceramint

Tuning the peak effect in the $Y_{1-x}Nd_xBa_2Cu_3O_{7-\delta}$ compound

D.M. Gokhfeld[a], D.A. Balaev[a,b], I.S. Yakimov[b], M.I. Petrov[a], S.V. Semenov[a,b,*]

[a] Kirensky Institute of Physics, Federal Research Center KSC SB RAS, Akademgorodok 50, Krasnoyarsk 660036, Russia
[b] Siberian Federal University, Krasnoyarsk 660041 Russia

ARTICLE INFO

Keywords:
Peak effect
Bulk superconductors
Critical current
Pinning
Characterization
YBCO

ABSTRACT

Polycrystalline $Y_{1-x}Nd_xBa_2Cu_3O_{7-\delta}$ (x=0.02, 0.11, and 0.25) superconductors are synthesized. Nd atoms are uniformly distributed over grains. The magnetization loops of the samples have a pronounced second peak in a wide temperature range. The magnetization data are analyzed using the extended critical state model. It is found that the order-disorder transition of the vortex lattice is affected by doping with neodymium and temperature; the second-peak field and width decrease monotonically with increasing x value. The undoped polycrystalline $YBa_2Cu_3O_{7-\delta}$ compound is assumed to exhibit the peak effect in higher magnetic fields.

1. Introduction

The critical current of type-II superconductors is determined by the magnetic flux pinning. The capability of current transfer can be considerably improved by using artificial structural defects, which work as pinning centers [1–3]. The structural defects can be embedded by admixing, doping, or irradiation. Different defects enhance the pinning in different magnetic field ranges and can give rise to the peak effect [3,4]. The peak effect consists in a counterintuitive growth of the critical current in a certain magnetic field range, which is accompanied by a fishtail peculiarity, i.e. the second peak in the forward and reverse branches of the magnetization loop. The peak effect is attributed to transitions of the Abrikosov vortex lattice [5,6] or to a phase separation [7,8].

The second peak is observed in the magnetization loops of bulk $YBa_2Cu_3O_{7-\delta}$ single crystals [5,9], while in the polycrystalline $YBa_2Cu_3O_{7-\delta}$ compound the peak effect is difficult to observe [10]. On the contrary, the magnetization loops of granular Nd- and Eu-based 1-2-3 superconductors contain the pronounced second peak corresponding to magnetic field H weaker than 50 kOe at temperatures above 10 K [10–12].

It is well-known that the critical current in the $YBa_2Cu_3O_{7-\delta}$ compounds can be increased by chemical substitution of rare-earth elements for Y [13–19] or Ba [20,21]. In addition, the peak effect in $YBa_2Cu_3O_{7-\delta}$ can be induced by doping with Nd [4,13,22,23].

It was demonstrated in many works that the peak maximum shifts upon temperature variation. However, other ways of shifting the second peak have not been investigated. In the present work, we study the second peak evolution in the $Y_{1-x}Nd_xBa_2Cu_3O_{7-\delta}$ compounds where Y is partially replaced by Nd.

This article is organized as follows. The experimental techniques used are outlined in Section 2. Sample characterization, including XRD and SEM studies and $M(T)$ and $R(T)$ measurements, is described in Section 3. Section 4 presents magnetization loops and magnetic field dependences of the critical current densities and pinning force densities obtained in the framework of the Bean model. In Section 4, we analyze the magnetization loops using the extended critical state model [24–26].

2. Experimental

A series of optimally doped $Y_{1-x}Nd_xBa_2Cu_3O_{7-\delta}$ (x=0.02, 0.11, and 0.25) samples was synthesized by the solid-state reactions technique. X-ray powder diffraction (XRD) data were obtained using Shimadzu XRD-7000S diffractometer (CuKα radiation). The 2θ angle ranged from 5° to 70° with a step of 0.02°. Scanning electron microscopy (SEM) and energy dispersive spectrometry (EDS) investigations of the synthesized samples were carried out using Hitachi TM 3000 microscope. To perform the resistive measurements, parallelepiped samples about 1×1×8 mm^3 in size were cut from the synthesized pellets.

* Corresponding author at: Kirensky Institute of Physics, Federal Research Center KSC SB RAS, Akademgorodok 50, Krasnoyarsk 660036, Russia.
E-mail address: svsemenov@iph.krasn.ru (S.V. Semenov).

http://dx.doi.org/10.1016/j.ceramint.2017.05.011
Received 28 March 2017; Received in revised form 24 April 2017; Accepted 2 May 2017

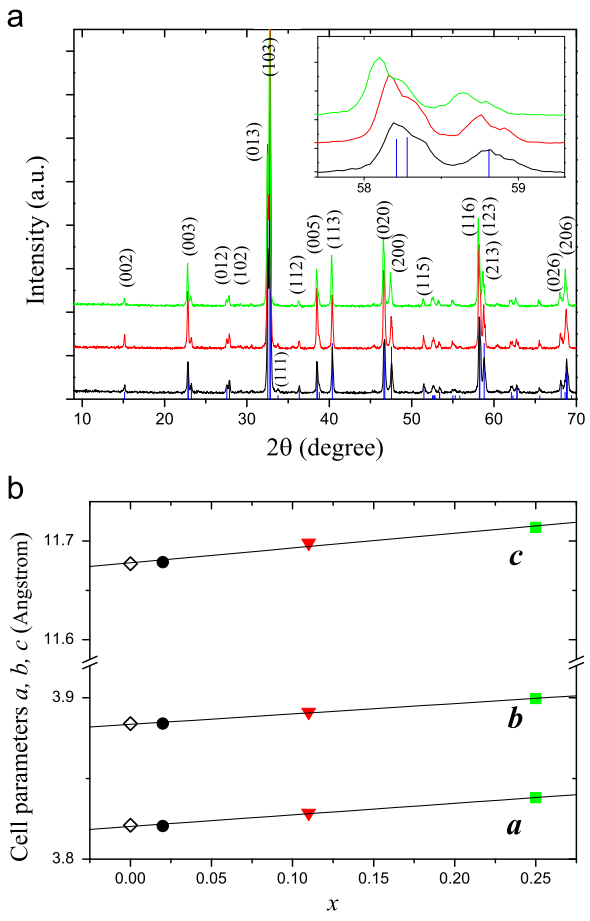

Fig. 1. (a) X-ray diffraction and (b) lattice parameters. For clarity, curves in Fig. 1a are shifted along the intensity axis. Lines in Fig. 1b are linear fits.

Temperature dependences of the resistivity ρ(*T*) were measured by the four-probe method using the transport current of 1 mA. Magnetic measurements were performed using Quantum Design PPMS-6000 vibrating sample magnetometer.

3. Sample characterization

3.1. X-ray diffraction

Fig. 1a shows XRD patterns of the synthesized samples. Blue vertical marks in Fig. 1a indicate the PDF2 ICDD reference pattern #71-5184. All the peaks are seen to correspond to the peaks in a reference pattern of the orthorhombic $YBa_2Cu_3O_{7-\delta}$ material. No signs of other phases are observed. For the samples with x=0.11 and 0.25, the peaks are noticeably shifted to the left relative to their positions in the reference pattern (see Insert on Fig. 1a). This shift is proportional to the Nd content x.

The crystal lattice parameters were determined by the full-profile analysis using the DDM software [27]. Fig. 1b demonstrates the a, b, c parameters of the samples with different x; open circles show the parameters of the reference pattern ($YBa_2Cu_3O_{7-\delta}$). Where no error bars are shown, the errors are less than the symbol size. Each of the parameters a, b, and c grows linearly with x. The linear dependence of the a, b, and c values on x indicates that Nd is completely dissolved in the $Y_{1-x}Nd_xBa_2Cu_3O_{7-\delta}$ compound.

The XRD results conclude that the substitution of Nd with the larger atomic radius for Y causes the lattice expansion in $Y_{1-x}Nd_xBa_2Cu_3O_{7-\delta}$ compound.

3.2. Microstructure

SEM images of the samples are shown in Fig. 2a–c. The samples have the disordered granular structure. It can be seen that the samples with x=0.11 and 0.25 consist of coarser grains and are less porous than the sample with x=0.02. The average grain size is ~2.5 μm at x=0.02 and ~4 μm at x=0.11 and 0.25.

Fig. 2d shows a typical EDS image of the sample with x=0.11. Analysis of the elemental composition based on EDS map spectra showed that in all the samples the element contents correspond to the nominal chemical formula of the compound. The EDS images confirm the uniform distribution of Nd atoms over grains.

3.3. Critical temperature and ρ(T) dependences

Fig. 3a shows temperature dependences of the magnetic moment $M(T)$ measured under zero field cooled (ZFC) and field cooled (FC) conditions in a magnetic field H of 10 Oe. The superconducting transition temperature T_c determined from these data is 92.5, 92.3, and 91.7 K for the samples with x=0.02, 0.11 and 0.25.

Fig. 3b shows the ρ(T) dependences of the samples. At temperatures above T_c, these dependences exhibit the metal-like behavior typical of the YBCO system. The onset of the resistive transition corresponds to the T_c values obtained from the $M(T)$ dependence. The insert in Fig. 3b shows the enlarged resistive transition. The two-step ρ(T) dependence near the superconducting transition is typical of granular high-T_c superconductors [28–30]. The sharp resistance drop corresponds to the superconducting transition of grains. The smooth part of the ρ(T) dependence reflects the transition in the grain boundary subsystem, which can be presented as a Josephson junction network. For all the samples, the temperature range of the smooth part is 1.5–1.8 K. This indicates that the substitution of Nd for Y in $Y_{1-x}Nd_xBa_2Cu_3O_{7-\delta}$ almost does not change the intergrain (Josephson) coupling in the samples with x≤0.25.

4. Results and discussion

4.1. Magnetization loops

Fig. 4a–e show magnetic hysteresis loops for the $Y_{1-x}Nd_xBa_2Cu_3O_{7-\delta}$ samples in the temperature range of 4.2–80 K. The $M(H)$ dependences are tilted anticlockwise and their tilt increases with the Nd concentration x. In addition, in high fields the fishtail feature (the second peak) is observed.

The tilt of the magnetization loops is apparently related to the superposition of the magnetization hysteresis $M_S(H)$ of superconductive grains and additional paramagnetic magnetization $M_P(H)$ [11,12]. The additional paramagnetic magnetization can be taken into account from the high-field portion of the magnetization loop. This paramagnetic magnetization is expressed as $M_P(H)=NgJ\mu_B B_J(gJ\mu_B\mu_0 H/k_BT)$, where N is the number of magnetic ions per unit volume, μ_B is the Bohr magneton, k_B is the Boltzmann constant, g is the Lande g factor, J is the angular momentum quantum number, and B_J is Brillouin function. The N value is chosen to obtain the superconducting magnetization loops $M_S(H)=M(H)-M_P(H)$, which are not tilted in high fields H. One of the magnetization loops $M_S(H)$ without the paramagnetic contribution is presented in Fig. 4f. We found that the N value increases with